Pattern Recognition 107 (2020) 107483

Contents lists available at ScienceDirect

Pattern Recognition

journal homepage: www.elsevier.com/locate/patcog

3DSymm: Robust and Accurate 3D Reflection Symmetry Detection

Rajendra Nagar[a,*], Shanmuganathan Raman[b]

[a] Assistant Professor, Department of Electrical Engineering, Indian Institute of Technology Jodhpur, Rajasthan, 342037, India
[b] Jibaben Patel Chair in Artificial Intelligence and Associate Professor, Electrical Engineering and Computer Science and Engineering, Indian Institute of Technology Gandhinagar, Gujarat, 382355, India

ARTICLE INFO

Article history:
Received 16 August 2019
Revised 19 May 2020
Accepted 31 May 2020
Available online 1 June 2020

Keywords:
Reflection symmetry
Point cloud
Optimization

ABSTRACT

Reflection symmetry is a very commonly occurring feature in both natural and man-made objects, which helps in understanding objects better and makes them visually pleasing. Detection of reflection symmetry is a fundamental problem in the field of computer vision and computer graphics which aids in understanding and representing reflective symmetric objects. In this work, we attempt the problem of detecting the 3D global reflection symmetry of a 3D object represented as a point cloud. The main challenge is to handle outliers, missing parts, and perturbations from the perfect reflection symmetry. We propose a descriptor-free approach, in which, we pose the problem of reflection symmetry detection as an optimization problem and provide a closed-form solution. We show that the proposed method achieves state-of-the-art performance on the standard dataset.

1. Introduction

There are three main types of symmetry present in the natural and man-made objects - reflection symmetry, rotational symmetry, and translational symmetry. Reflection symmetry is the most frequently occurring symmetry in natural and man-made objects. Objects can be represented as digital images or 3D point clouds. The primary motivation for detecting reflection symmetry in 3D point clouds is the following. There are various applications such as 3D surface reconstruction [1], model completion [1–3], symmetrization [4], model reduction [5], 3D model reconstruction from a single image [6], symmetric object segmentation and recognition [7–11], and viewpoint selection [12]. These applications require robust, fast, and accurate detection of 3D reflection symmetry for further processing.

The problem of detecting reflection symmetry is an example of the pattern recognition problem where our goal is to find the repetitive patterns present in the images or 3D point class. For example, in an image containing reflective symmetric objects, object pixels appear two times with respect to the symmetry axis, while in an image containing translational symmetric objects, object pixels appear multiple times at the grid corners. The primary challenge is to estimate the reflection symmetry or detecting the reflection symmetry pattern in the presence of outlier points, missing parts of the symmetric objects, and deviations from the perfect reflection symmetry. The problem of detecting the reflection symmetry of an object amounts to solving the following two sub-problems - (a) determining the plane of reflection symmetry and (b) finding correspondences between the reflective symmetric points. There exist several approaches for detecting symmetry in 3D point clouds [13]. However, these methods do not scale well with the size of the input point cloud and can not handle a large number of outliers, missing parts, and deviations from the perfect symmetry. For example, a recent method proposed in [14] solves an integer linear program that prohibits it from being used to find symmetry in large point clouds. The method proposed in [15] is not robust to the outliers.

We pose the problem of reflection symmetry detection as an optimization problem by using the reflection symmetry transformation proposed in [14]. We parametrize the plane of reflection symmetry using a rotation matrix and a translation vector and represent the correspondences between the reflective symmetric points using a permutation matrix. We solve the proposed optimization problem for the reflection matrix, the translation vector, and the permutation matrix. The main challenge lies in the fact that the proposed optimization problem is non-linear and non-convex in the reflection matrix and NP-hard in the estimation of correspondences between the reflective symmetric points. There are impurities present in the input point cloud, such as outliers, missing parts, and deviation from symmetry, which further make this problem hard to solve. We propose a fast randomized algorithm to initialize the reflection matrix such that the estimated reflection matrix is in the proximity of the global minimum. We

* Corresponding author.
E-mail addresses: rn@iitj.ac.in (R. Nagar), shanmuga@iitgn.ac.in (S. Raman).

https://doi.org/10.1016/j.patcog.2020.107483
0031-3203/

also initialize the translation vector as the mean of the input point cloud using the fact that the reflection symmetry plane of an object passes through the center of mass of the object. We use the reflection matrix and the translation vector to estimate the symmetric correspondences. Then, we update the reflection matrix and the translation vector using these correspondences. We iteratively repeat this procedure until convergence.

The proposed approach depends only on the geometry of the input point cloud and does not use any feature descriptor. Therefore, our approach can be applied to data of any form such as point cloud sampled from the surface of the symmetric object and the volumetric point cloud. This is advantageous since all the descriptors might not be invariant to the outliers and the type of descriptor used also depends on the form of the input point cloud.

Our main contributions are the following.

- We formulate the problem of detecting reflection symmetry as an optimization problem to find the global reflection symmetry in both the volumetric point cloud and the point cloud sampled from the surface of an object in the presence of outliers, perturbation from the perfect symmetry, and missing parts.
- We empirically show that the proposed optimization problem is a non-linear and non-convex problem and provides a fast descriptor-free randomized algorithm to initialize the reflection symmetry plane. We also give a theoretical understanding for 2-dimensional point clouds.
- We provide a closed-form solution to the problem of estimating the global 3D reflection symmetry plane.

The rest of the paper is organized as follows. In Section 2, we review the literature corresponding to the 3D reflection symmetry. In Section 3, we formulate the problem of detecting global reflection symmetry in point clouds as an optimization problem. In Sections 4 and 5, we discuss the proposed solution for this optimization problem. In Section 6, we present results and comparisons with the state-of-the-art methods on the benchmark dataset. In Section 7, we conclude our approach and discuss future directions.

2. Related work

The problem of reflection symmetry detection in objects represented by 3D point clouds has been an active topic of research in computer vision, computer graphics, and pattern recognition for a long time. The survey paper in [16] reviewed the 2D symmetry detection algorithms and the state-of-the-art report in [17] reviewed the 3D symmetry detection algorithms.

There exist several approaches that automatically detect the plane of reflection symmetry in point clouds without using features. Lipman et al. in [18] and Xu et al. in [19] find correspondences between the reflective symmetric points without using feature descriptors. However, both the methods depend on the choice of a hyper-parameter to detect the reflection symmetry in the perturbed patterns and the bad choice of this hyper-parameter can lead to a higher computation time. Zabrodsky et al. find the plane of reflection symmetry in a set of points in $\mathbb{R}^2$ which needs point correspondences computed in advance [20]. Authors in the work [14] proposed a manifold optimization-based approach detecting approximate reflection symmetry of d-dimensional point clouds. The method proposed in [21] only detects symmetry in the planar point clouds. The method proposed in [22] uses multiple viewpoints of a 3D model to detect the plane of reflection symmetry. Whereas, our approach can detect symmetry using only one viewpoint. The method proposed in [23] automatically detects the plane of reflection symmetry. However, it requires many parameters to be initialized and it is a computationally expensive method.

The methods proposed in the works [1,5] and [24] used surface features such as curvature to find reflection symmetry. However, features in the presence of outliers and missing parts are not reliable. Authors in the work [25] used the generalized moment functions. Authors in the work [26] detectedsymmetry by constructing a graph based on slippage features. Authors in the works [27] and [28] used image features to detect symmetry in the structure from the motion pipeline which highly relies on the underlying images. Authors in the work [15] proposed a registration (iterative closest point (ICP) [29,30]) based approach. They reflected the input point cloud about an arbitrary plane and registered the original and the reflected point clouds. However, it suffered from the initialization problem and is not robust to the outliers. Ecins et al. proposed a symmetrical fitting based approach which is not robust to the outliers and the missing parts [13]. Both these methods [15] and [13] pose the problem of symmetry detection as a registration problem which increases the number of parameters of the transformation matrix. Nagar and Raman posed the reflection symmetry problem as an optimization problem which they solved using the manifold optimization technique [14]. This method works well for the approximate symmetries but less robust to outliers and missing parts. Furthermore, it has high computational complexity due to the use of an integer linear program.

There are various exciting approaches that use surface features to detect symmetry such as [31–33]. For example, the method proposed in [34] uses line features on a generated graph and the method proposed in [35] uses extended Gaussian images to detect the reflection symmetry. However, these approaches can not directly be adapted to work on volumetric point clouds. There exist several methods that use mesh connectivity to find the intrinsic symmetry and assume that the points are sampled from the surface of 2-manifolds. For example the methods in [36] and [37] used eigenfunction of the Laplace-Beltrami operator, the method in [38] uses the functional map framework, the method in [39] used heat kernel signatures, the method in [40] uses Mobius transformation to detect intrinsic symmetry. However, these methods can not be used to detect extrinsic symmetry in the point clouds as they rely on the point connectivity and assume that the shape represents a 2-manifold. In [41–46], authors proposed detecting symmetry in images. The symmetry detection problem in real-world images also is an active research problem [47]. For example, the methods proposed in [48] and [49] use gradient information, the method in [50] uses spectral clustering, the method proposed in [51] uses edge orientation of objects, the method proposed in [52] local appearance structural descriptors, and [53] use texture and gradient information to detect the reflection symmetry axes present in the input image. However, these methods can not be directly extended to point clouds. Furthermore, these approaches rely on accurate feature descriptors.

3. Problem formulation

Let $\mathcal{P} = \{\mathbf{p}_1, \mathbf{p}_2, \ldots, \mathbf{p}_n\}$ be the input point cloud with n points and represented by a matrix $\mathbf{P} = \begin{bmatrix}\mathbf{p}_1 & \mathbf{p}_2 & \ldots & \mathbf{p}_n\end{bmatrix} \in \mathbb{R}^{3\times n}$. As proposed in [14], the reflection of a point about a given symmetry axis is obtained by translating the origin of the coordinate system on the symmetry axis and then by rotating it such that the x-axis is aligned with the symmetry axis. Then, we negate the y-coordinate of the point and rotate back the coordinate system to the original position. A similar sequence of transformations is followed in the 3D space.

More formally, if $\mathbf{p}_j$ is the reflection of the point $\mathbf{p}_i$, then we can represent this whole procedure as follows.

$$\mathbf{p}_j = \mathbf{R}_{\theta_x}^{\top}\mathbf{R}_{\theta_y}^{\top}\mathbf{Q}\mathbf{R}_{\theta_y}\mathbf{R}_{\theta_x}(\mathbf{p}_i - \mathbf{c}) + \mathbf{c}. \tag{1}$$

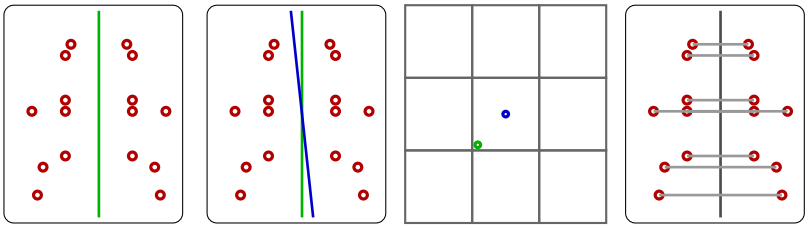

Fig. 1. Key steps of our approach. (a) Input point cloud with reflection symmetry shown in light-green color. (b) We first estimate the reflection symmetry, shown in light-blue color, using a randomized initialization strategy and discrete initialization of parameter. (c) The green color point represents the true reflection symmetry and the blue point represents the initialized reflection symmetry. (d) The obtained reflection symmetry axis and the pairs of reflective symmetric points using the proposed approach. (For interpretation of the references to colour in this figure legend, the reader is referred to the web version of this article.)

Here, the matrices $\mathbf{R}_{\theta_x}$ and $\mathbf{R}_{\theta_y}$ represent the rotation matrices by the angle θ_x about x-axis and by the angle θ_y about the y-axis, respectively. The variable $\mathbf{c}$ is a point on the plane of reflection symmetry. The matrix $\mathbf{Q} = \begin{bmatrix} \mathbf{I}_2 & \mathbf{0}_2 \\ \mathbf{0}_2^\top & -1 \end{bmatrix}$ negates the z-coordinate of a point. Here, $\mathbf{I}_2$ is the 2×2 identity matrix and $\mathbf{0}_2$ is the zero vector of size 2×1. Now, let $\mathbf{R} = \mathbf{R}_{\theta_y}\mathbf{R}_{\theta_x}$, then $\mathbf{p}_j = \mathbf{R}^\top\mathbf{Q}\mathbf{R}(\mathbf{p}_i - \mathbf{c}) + \mathbf{c}$. Therefore, given the input point cloud $\mathcal{P}$, our goal is to find the reflection symmetry transformation matrices $\mathbf{R}_{\theta_x}$, $\mathbf{R}_{\theta_y}$, $\mathbf{c}$, and all the pairs $(\mathbf{p}_i, \mathbf{p}_j)$ of reflective symmetric points. We formulate the problem of finding the reflection symmetry in an optimization framework as follows. For each pair $(\mathbf{p}_i, \mathbf{p}_j)$ of reflective symmetric points, we want $\mathbf{p}_j = \mathbf{R}^\top\mathbf{Q}\mathbf{R}(\mathbf{p}_i - \mathbf{c}) + \mathbf{c}$. However in practice, this equality does not hold true due to perturbations from the perfect symmetry. Therefore, we want the error $\|\mathbf{R}^\top\mathbf{Q}\mathbf{R}(\mathbf{p}_i - \mathbf{c}) + \mathbf{c} - \mathbf{p}_j\|_2^2$ to be as small as possible. Therefore, we want the error $\sum_{i\in[n]} \|\mathbf{R}^\top\mathbf{Q}\mathbf{R}(\mathbf{p}_i - \mathbf{c}) + \mathbf{c} - \mathbf{p}_j\|_2^2$ to be minimized with respect to $\mathbf{R}$, $\mathbf{c}$, and all the pairs $(\mathbf{p}_i, \mathbf{p}_j)$. Here, $[n] = \{1, 2, \ldots, n\}$. Thus, our goal is to solve the optimization problem defined in the below equation.

$$\underset{\substack{\mathbf{R},\mathbf{c},\\ (i,j),\forall i\in[n]}}{\arg\min} \quad \sum_{i\in[n]} \left\|\mathbf{R}^\top\mathbf{Q}\mathbf{R}(\mathbf{p}_i - \mathbf{c}) + \mathbf{c} - \mathbf{p}_j\right\|_2^2$$
$$\text{subject to } \mathbf{R}^\top\mathbf{R} = \mathbf{I}, \det(\mathbf{R}) = 1, \mathbf{R} \in \mathbb{R}^{3\times3}, \mathbf{c} \in \mathbb{R}^3. \tag{2}$$

In Fig. 1, we show the key steps of our approach which we discuss in Section 4.

4. Proposed approach

In order to solve the optimization problem defined in Eq. (2), we follow the following alternating optimization approach. We first initialize the reflection matrices $\mathbf{R}$, $\mathbf{c}$, and find the pairs of reflective symmetric points. We then update the reflection symmetry matrices $\mathbf{R}$ and $\mathbf{c}$. We again update the mirror image of each point. We iteratively repeat this process until there are no further changes in $\mathbf{R}$, $\mathbf{c}$, and the mirror image of each point. First, we rewrite the optimization problem defined in Eq. (2) in a more convenient form as follows.

Let us denote the correspondences between the reflective symmetric points by the matrix $\mathbf{\Pi} \in \{0, 1\}^{n\times n}$, such that $\mathbf{\Pi}(i, j) = \mathbf{\Pi}(j, i) = 1$, if $\mathbf{p}_j = \mathbf{R}^\top\mathbf{Q}\mathbf{R}(\mathbf{p}_i - \mathbf{c}) + \mathbf{c}$ and $\mathbf{\Pi}(i, j) = \mathbf{\Pi}(j, i) = 0$, otherwise. We further let $\mathbf{S} = \mathbf{R}^\top\mathbf{Q}\mathbf{R}$. The matrices $\mathbf{R}$ and $\mathbf{Q}$ are orthogonal matrices and the determinant of the matrix $\mathbf{Q}$ is equal to -1. Therefore, the matrix $\mathbf{S}$ is an orthogonal matrix with determinant equal to -1. We observe that the matrix $\mathbf{\Pi}$ is a permutation matrix. Further, since the plane of reflection symmetry passes through the center of mass of the object and the point $\mathbf{c}$ is any point on the plane of reflection symmetry. Therefore, we center the input point cloud to have $\mathbf{c} = \mathbf{0}$ by subtracting the mean. Now, the optimization problem defined in Eq. (2) can be reformulated as below.

$$\underset{\mathbf{\Pi}\in\{0,1\}^{n\times n},\mathbf{S}\in\mathbb{R}^{3\times3},\mathbf{c}\in\mathbb{R}^3}{\arg\min} \quad \left\|\mathbf{S}(\mathbf{P} - \mathbf{c}\mathbf{1}^\top) + \mathbf{c}\mathbf{1}^\top - \mathbf{P}\mathbf{\Pi}\right\|_{\mathrm{F}}^2$$
$$\text{subject to} \quad \mathbf{S}^\top\mathbf{S} = \mathbf{I}, \det(\mathbf{S}) = -1. \tag{3}$$

Here, $\mathbf{1}$ is vector of size $n \times 1$ with all the elements equal to 1.

4.1. Fix $\mathbf{\Pi}$, $\mathbf{c}$ and estimate the optimal $\mathbf{S}$

In order to find the reflection matrix $\mathbf{S}$, we fix the matrix $\mathbf{\Pi}$ and minimize the problem in Eq. (3) with respect to the matrix $\mathbf{S}$. We derive a closed-form solution for the matrix $\mathbf{S}$ as follows. We can rewrite the optimization problem in Eq. (3) for optimizing it with respect to $\mathbf{S}$ as $\max_{\mathbf{S}} \text{trace}((\mathbf{P} - \mathbf{c}\mathbf{1}^\top)^\top\mathbf{S}(\mathbf{P}\mathbf{\Pi} - \mathbf{c}\mathbf{1}^\top))$. This can be further modified using the property of trace as below.

$$\max_{\mathbf{S}} \text{trace}(\mathbf{S}(\mathbf{P}\mathbf{\Pi} - \mathbf{c}\mathbf{1}^\top)(\mathbf{P} - \mathbf{c}\mathbf{1}^\top)^\top). \tag{4}$$

Now, let $\mathbf{W} = (\mathbf{P}\mathbf{\Pi} - \mathbf{c}\mathbf{1}^\top)(\mathbf{P} - \mathbf{c}\mathbf{1}^\top)^\top$ be a matrix and $\mathbf{W} = \mathbf{U}\mathbf{\Sigma}\mathbf{V}^\top$ be the singular value decomposition of the matrix $\mathbf{W}$. Then, we have that $\max_{\mathbf{S}} \text{trace}(\mathbf{S}\mathbf{U}\mathbf{\Sigma}\mathbf{V}^\top) = \max_{\mathbf{S}} \text{trace}(\mathbf{\Sigma}\mathbf{V}^\top\mathbf{S}\mathbf{U})$. Since the matrices $\mathbf{S}$, $\mathbf{U}$, and $\mathbf{V}$ are orthogonal matrices, $\mathbf{V}^\top\mathbf{S}\mathbf{U}$ is also an orthogonal matrix. Now, according to Sorkine and Alexa [54] and Arun et al. [55], the optimal solution $\mathbf{S}^\star$ to this problem satisfies the condition $\mathbf{S}^\star = \mathbf{U}\mathbf{V}^\top$ with determinant equal to -1.

4.2. Fix $\mathbf{R}$, $\mathbf{\Pi}$ and estimate the optimal $\mathbf{c}$

In order to find the optimal $\mathbf{c}$, we fix the rotation matrix $\mathbf{R}$ and the symmetric correspondences matrix $\mathbf{\Pi}$. We minimize the optimization problem in Eq. (3) with respect to $\mathbf{c}$. Let us rewrite the error function as $\|\mathbf{A} - \mathbf{B}\mathbf{c}\mathbf{1}^\top\|_{\mathrm{F}}^2$. Here, $\mathbf{A} = \mathbf{S}\mathbf{P} - \mathbf{P}\mathbf{\Pi}$ and $\mathbf{B} = \mathbf{S} - \mathbf{I}$. Now, in order to find the optimal point, we set the gradient $-2\mathbf{B}^\top\mathbf{A}\mathbf{1} - 4\mathbf{B}\mathbf{c}\mathbf{1}^\top\mathbf{1}$ of the error function with respect to $\mathbf{c}$ equal to $\mathbf{0}$. Therefore,

$$\mathbf{B}\mathbf{c}^\star = \frac{1}{2n}\mathbf{B}^\top\mathbf{A}\mathbf{1}. \tag{5}$$

We further show that the function $f(\mathbf{R}, \mathbf{c}, \mathbf{\Pi}) = \left\|\mathbf{S}(\mathbf{P} - \mathbf{c}\mathbf{1}^\top) + \mathbf{c}\mathbf{1}^\top - \mathbf{P}\mathbf{\Pi}\right\|_{\mathrm{F}}^2$ is convex in $\mathbf{c}$. Therefore, $\mathbf{c}^\star$ is the global minimizer. We show it by proving that the Hessian matrix is a positive semi-definite matrix.

Claim: *The Hessian matrix* $\mathbf{H}$ *of the cost function with respect to* $\mathbf{c}$, *which is equal to* $4n(\mathbf{I} - \mathbf{S})$, *is a positive semi-definite matrix.*

Proof. Consider the scalar $\mathbf{x}^\top\mathbf{H}\mathbf{x}, \forall\mathbf{x} \in \mathbb{R}^3$. We have that $\mathbf{x}^\top\mathbf{H}\mathbf{x} = 4n\mathbf{x}^\top(\mathbf{I} - \mathbf{S})\mathbf{x} = 4n\mathbf{x}^\top(\mathbf{I} - \mathbf{R}^\top\mathbf{Q}\mathbf{R})\mathbf{x} = 4n\|\mathbf{x}\|_2^2 - 4n\mathbf{x}^\top\mathbf{R}^\top\mathbf{Q}\mathbf{R}\mathbf{x} = 4n\|\mathbf{x}\|_2^2 - 4n(\mathbf{R}\mathbf{x})^\top\mathbf{Q}\mathbf{R}\mathbf{x}$. Now, let $\mathbf{y} = \mathbf{R}\mathbf{x}$. Since $\mathbf{R}$ is a rotation matrix, we have $\|\mathbf{y}\|_2^2 = \|\mathbf{x}\|_2^2$. Therefore, $\mathbf{x}^\top\mathbf{H}_\mathbf{c}\mathbf{x} = 4n(x_1^2 + x_2^2 + x_3^2) - 4n(y_1^2 + y_2^2 - y_3^2) = 4n(x_1^2 + x_2^2 + x_3^2) - 4n(x_1^2 + x_2^2 + x_3^2 - y_3^2 - y_3^2) = 8y_3^2 \geq 0$. Hence, the Hessian matrix is a positive semi-definite matrix. Therefore, the function f is convex in $\mathbf{c}$. □

4.3. Fix $\mathbf{R}$, c and estimate the optimal $\mathbf{\Pi}$

The correspondences matrix $\mathbf{\Pi}$ is a binary matrix and the problem of finding the exact $\mathbf{\Pi}$ amounts to solving an integer linear program which is an NP-hard problem. Instead, we find the approximate $\mathbf{\Pi}$ using the nearest neighbor approach as follows. Let us define the matrix containing the reflected points as columns to be $\mathbf{P}_r = \mathbf{S}(\mathbf{P} - \mathbf{c}\mathbf{1}^\top) + \mathbf{c}\mathbf{1}^\top$. Then, we shall define the mirror reflection point for the point $\mathbf{p}_i$ as the nearest column from the columns of the matrix $\mathbf{P}_r$. After finding the approximate reflection points, we further keep only the pairs such that if the reflection point of the point $\mathbf{p}_i$ is the point $\mathbf{p}_j$, and vice versa. Now, we show that the cost function f is a non-linear and a non-convex function. Therefore, we need an initialization close to the optimal solution. We propose a fast randomized algorithm to search for a good initialization.

5. Initialization strategy

We have seen that there exists a closed form solution for **S, c** is the solution of a linear system, and the matrix $\mathbf{\Pi}$ can be approximated by a nearest neighbor approach. We have proposed an alternating framework where we fix other variables and optimize with respect to one variable. The core problem of this alternating strategy is the initialization. There are two possibilities: (a) initializing the correspondences matrix $\mathbf{\Pi}$ and (b) initializing the reflection symmetry parameter **S**.

Initialize $\mathbf{\Pi}$: This is an intractable problem since the possible permutation matrices $\mathbf{\Pi}$ are $\frac{n}{2}!$. Even for hundred points, there will be 3.0414093×10^{64} permutation matrices.

Initialize S: This is a more feasible approach as we show below. Let us parameterize the space of all orthogonal matrices with determinants equal to -1. We have seen that $\mathbf{S} = \mathbf{R}^\top\mathbf{Q}\mathbf{R}$, where $\mathbf{R}$ is an orthogonal matrix with determinant equal to $+1$. The matrix $\mathbf{R} = \mathbf{R}_{\theta_x}\mathbf{R}_{\theta_y}$ represents the rotation about the y-axis by an angle of θ_y followed by the rotation about the x-axis by an angle of θ_x. Therefore, the space of all matrices $\mathbf{S}$ is parameterized by the parameters θ_x and θ_y, such that $\theta_x, \theta_y \in [-90^\circ, +90^\circ]$. Although the domain $[-90^\circ, +90^\circ] \times [-90^\circ, +90^\circ]$ has infinitely many points to try, we show the following result.

Result 1. *Let the point $\boldsymbol{\theta}^\star = [\theta_x^\star\ \theta_y^\star]^\top$ be the global minimizer of the cost function $f(\boldsymbol{\theta}) = \left\|\mathbf{S}(\theta_x, \theta_y)(\mathbf{P} - \mathbf{c}\mathbf{1}^\top) + \mathbf{c}\mathbf{1}^\top - \mathbf{P}\mathbf{\Pi}\right\|_F^2$. Then $f(\boldsymbol{\theta}) \geq f(\boldsymbol{\theta}^\star)$, $\forall \boldsymbol{\theta} \in [\theta_x - \phi, \theta_x + \phi] \times [\theta_y - \phi, \theta_y + \phi]$ for some angle ϕ.*

We empirically show that the approximate value of ϕ is around 10°. Therefore, we try only for 100 points of the set $[-90^\circ, +90^\circ] \times [-90^\circ, +90^\circ]$. Now, we empirically find the value of the angle ϕ. We perform the following two experiments. First, we construct $n_1 = 10000$ point clouds $\mathcal{P}$ with each containing 5000 points with known ground truth symmetry planes and the correspondences between the reflective symmetric points are defined using Eq. (1).

Experiment 1. In the first experiment, we empirically find the diameter of the set (in the space of rotation angles) around the global minimum $[\theta_x^\star\ \theta_y^\star]^\top$ such that if we initialize the rotation angles in this set, then our method converges to $[\theta_x^\star\ \theta_y^\star]^\top$. More formally, we find the diameter of the set defined as below

$$\mathcal{S}_i = \left\{\boldsymbol{\theta}_i^0 \in [-90^\circ, 90^\circ] \times [-90^\circ, 90^\circ] : \| \boldsymbol{\theta}_c^i - \boldsymbol{\theta}_g^i\|_2 = 0^\circ\right\}, \forall i \in [n_1] \quad (6)$$

Here, $\boldsymbol{\theta}_i^0 = [\theta_x^0\ \theta_y^0]^\top$ is the initialization point for our approach, $\boldsymbol{\theta}_c^i$ is the optimal solution returned by our approach, and $\boldsymbol{\theta}_g^i$ is the global minimum for the ith point cloud. In Fig. 2, we show the average error $\frac{1}{n_1}\sum_{i=1}^{n_1} \|\boldsymbol{\theta}_c^i - \boldsymbol{\theta}_g^i\|_2$ vs the initialization angles θ_x and θ_y. We circularly shift the error $\|\boldsymbol{\theta}_c^i - \boldsymbol{\theta}_g^i\|_2$, so that the global minimum is 0°, $\forall i$, to find the average of these errors. We observe that $\|\boldsymbol{\theta}_c^i - \boldsymbol{\theta}_g^i\|_2 = 0^\circ$, if $\boldsymbol{\theta}_i^0 \in [-10^\circ, 10^\circ] \times [-10^\circ, 10^\circ]$.

Experiment 2. In the second experiment, we find the following two errors:

$e_i(\theta_x) = f(\mathbf{S}(\theta_x, \theta_y^i), \mathbf{c}^i, \mathbf{\Pi}^i), \theta_x \in [-90^\circ, +90^\circ],\ i \in \{1, \ldots, n_1\}$

and $e_i(\theta_y) = f(\mathbf{S}(\theta_x^i, \theta_y), \mathbf{c}^i, \mathbf{\Pi}^i), \theta_y \in [-90, +90],\ i \in \{1, \ldots, n_1\}$.

Here, $\theta_x^i, \theta_y^i, \mathbf{c}^i$, and $\mathbf{\Pi}^i$ are the ground-truth variables for the ith point cloud. In Fig. 3, we plot the average error $e_{me} = \frac{1}{n_1}\sum_{i=1}^{n_1} e_i$, the upper bound error $e_{ub} = \max(e_1, \ldots, e_{n_1})$, and the lower bound error $e_{lb} = \min(e_1, \ldots, e_{n_1})$. We circularly shift the error e_i so that the global minimum is 0°, $\forall i$, to find these errors. We observe that e_{me}, e_{ub}, and e_{lb} are non-linear and non-convex and in the region $(\theta_x, \theta_y) \in [\theta_x^\star - 10^\circ, \theta_x^\star + 10^\circ] \times [\theta_y^\star - 10^\circ, \theta_y^\star + 10^\circ]$, the point $(\theta_x^\star, \theta_x^\star)$ is the only local minimum point.

Theoretical Aspects: Without loss of generality, we show that the cost function is locally convex around the optimal solution for the case of 2D point clouds. We assume that the center of mass of the point cloud at the origin. Let, $\mathbf{P} = \begin{bmatrix}\mathbf{p}_1 & \mathbf{p}_2 & \cdots \mathbf{p}_n\end{bmatrix} \in \mathbf{R}^{2\times n}$ be the matrix representing n points. If θ is the parameter representing the slope of the reflection symmetry line. Then, we have that

$$\begin{aligned}\mathbf{p}_j &= \begin{bmatrix}\cos\theta & -\sin\theta\\ \sin\theta & \cos\theta\end{bmatrix}\begin{bmatrix}1 & 0\\ 0 & -1\end{bmatrix}\begin{bmatrix}\cos\theta & \sin\theta\\ -\sin\theta & \cos\theta\end{bmatrix}\mathbf{p}_i.\\ &= \mathbf{R}\mathbf{Q}\mathbf{R}^\top\mathbf{p}_i\\ &= \mathbf{S}\mathbf{p}_i. \end{aligned} \quad (7)$$

As shown in Section 4, the problem of finding the reflection symmetry plane, which is determined by the matrix $\mathbf{R}$, is equivalent to minimizing the error $f(\theta) = \text{trace}(\mathbf{S}\mathbf{W})$, where $\mathbf{W} = \mathbf{P}\mathbf{\Pi}\mathbf{P}^\top$. Now, we can simplify the function $f(\theta)$ as below.

$$\begin{aligned} f(\theta) &= -\text{trace}(\mathbf{S}\mathbf{W})\\ &= -\text{trace}\left(\begin{bmatrix}\cos 2\theta & \sin 2\theta\\ \sin 2\theta & -\cos 2\theta\end{bmatrix}\begin{bmatrix}w_1 & w_2\\ w_2 & w_3\end{bmatrix}\right)\\ &= -(w_1 - w_3)\cos 2\theta - 2w_2 \sin 2\theta. \end{aligned} \quad (8)$$

Therefore, we have to show that the error function $f(\theta) = -(w_1 - w_3)\cos 2\theta - 2w_2 \sin 2\theta$ is convex in the proximity of the optimal reflection angle $\theta^\star$. In order to show this, we analyze the values of the second derivative $f''(\theta)$ of the function $f(\theta)$. It can easily verified that $f''(\theta) = \cos(2\theta - \phi)$ and $f(\theta) = -\cos(2\theta - \phi)$. Here, $\phi = \tan^{-1}\left(\frac{2w_2}{w_1 - w_2}\right)$. Therefore, we have that $f''(\theta) = -f(\theta)$. Hence, both the functions $f(\theta)$ and $f''(\theta)$ have the same set of roots and are anti-phase of each others. Further, the function $f''(\theta)$ is always positive between the roots. Therefore, the function $f(\theta)$ is locally convex in the neighborhood of the optimal solution. In Fig. 4, we show this graphically.

Randomized Initialization. The plane of reflective symmetry passes through the center of mass of the input point cloud. Therefore, we initialize $\mathbf{c} = \frac{1}{n}\sum_{i=1}^{n}\mathbf{p}_i$. We have observed that if the initialization angles $\begin{bmatrix}\theta_x^0 & \theta_y^0\end{bmatrix}^\top$ of our approach are such that $\begin{bmatrix}\theta_x^0 & \theta_y^0\end{bmatrix}^\top \in \mathcal{D}$, then the optimal solution achieved by our approach converges to the global solution $\begin{bmatrix}\theta_x^\star & \theta_y^\star\end{bmatrix}^\top$. Here, $\mathcal{D} = [\theta_x^\star - 10^\circ, \theta_x^\star + 10^\circ] \times [\theta_y^\star - 10^\circ, \theta_y^\star + 10^\circ]$. Therefore, we find the approximate global minimum of the function f on the quantized domain or the grid domain as below.

$$\begin{aligned}\mathcal{G} = &\{-90^\circ, -70^\circ, \ldots, +70^\circ, +90^\circ\}\\ &\times\{-90^\circ, -70^\circ, \ldots, +70^\circ, +90^\circ\}. \end{aligned} \quad (9)$$

The size of the input set may be very large. Therefore, evaluating the function f on all the points of the grid $\mathcal{G}$ can be a time consuming step. Hence, we propose the following randomized algorithm. We choose a subset $\mathcal{P}_s$ of points from the set $\mathcal{P}$ uniformly at random such that $|\mathcal{P}_s| = n_2$. Then, we find the error $||(\mathbf{S}(\theta_x, \theta_y))(\mathbf{P}_s - \mathbf{c}\mathbf{1}^\top) + \mathbf{c}\mathbf{1}^\top - \mathbf{P}_s\mathbf{\Pi}_s||_F$, for each $(\theta_x, \theta_y) \in \mathcal{G}$. We choose the pair (θ_x, θ_y) for which the error is minimum. In

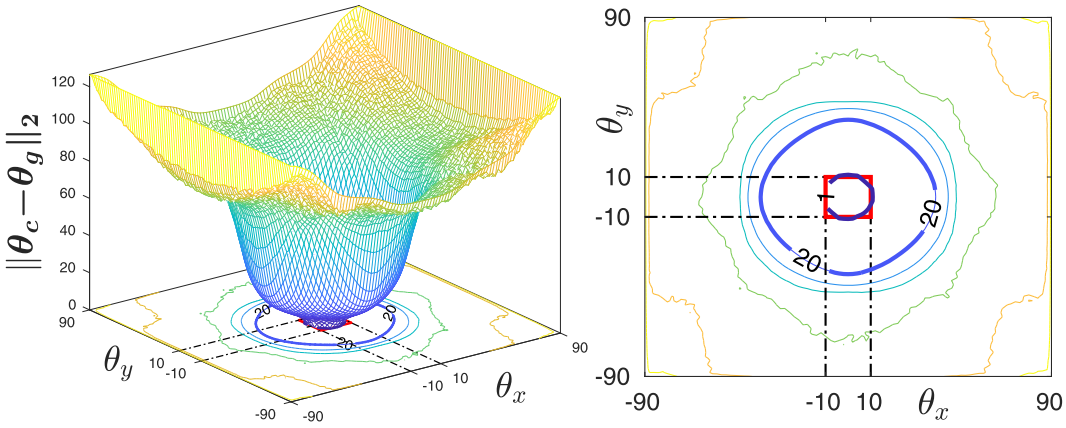

Fig. 2. (a) Distance of the optimal solution $\boldsymbol{\theta_g}$ from the solution $\boldsymbol{\theta_c}$ obtained by the proposed approach if initialized with the angle $\boldsymbol{\theta^0} = [\theta_x\ \theta_y]^\top$. (b) We observe that the distance $\|\boldsymbol{\theta}_c^i - \boldsymbol{\theta}_g^i\|_2 = 0^\circ$ if the initialization angles $[\theta_x\ \theta_y]^\top \in [-10^\circ, 10^\circ] \times [-10^\circ, 10^\circ]$.

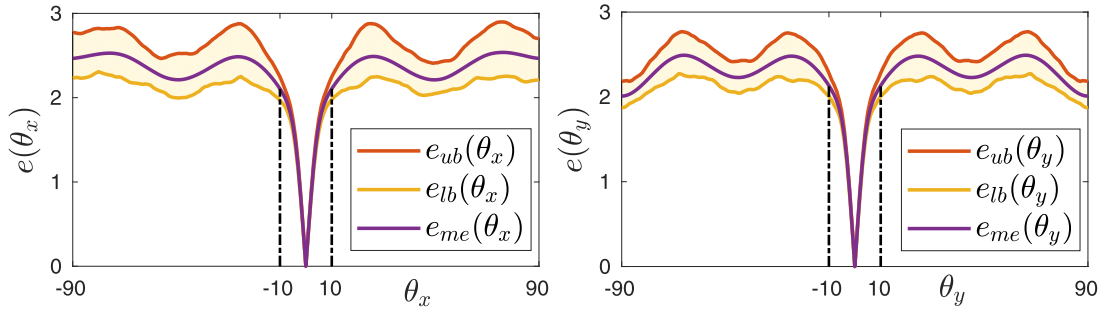

Fig. 3. Illustration of non-convexity of f. The average errors $e_{me}(\theta_x)$, $e_{me}(\theta_y)$, the upper bound errors $e_{ub}(\theta_x)$, $e_{ub}(\theta_x)$, and the lower bound errors $e_{lb}(\theta_x)$, $e_{lb}(\theta_x)$ vs θ_x and θ_y, respectively.

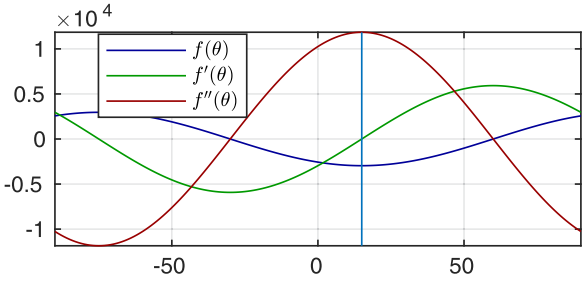

Fig. 4. The plot of the function $f(\theta)$, $f'(\theta)$, and $f''(\theta)$. We observe that $f''(\theta) > 0$ around the optimal solution.

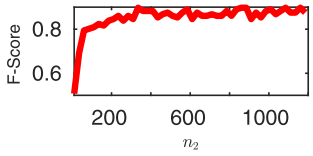

Fig. 5. Detected plane of reflection symmetry using the proposed approach in the scan of a real-world object from Funk et al. [47].

Algorithm 1 *Initializing reflection symmetry plane.*

Input: Point cloud $\mathcal{P}$ represented as a matrix $\mathbf{P} = \begin{bmatrix}\mathbf{p}_1 & \mathbf{p}_2 & \dots & \mathbf{p}_n\end{bmatrix} \in \mathbb{R}^{3\times n}$.

Steps Involved:

Form the grid $\mathcal{G} = \{-90^\circ, -70^\circ, \dots, +70^\circ, +90^\circ\} \times \{-90^\circ, -70^\circ, \dots, +70^\circ, +90^\circ\}$.
$\mathbf{C} \leftarrow \{0\}^{10\times 10}$.
Construct $\mathbf{P}_s$ by sampling n_2 columns uniformly at random of $\mathbf{P}$.
$\mathbf{c}_s \leftarrow \text{median}(\mathbf{P}_s)$.
for each $(s,t) \in \{1,\dots,10\} \times \{1,\dots,10\}$ **do**
  $(\theta_x, \theta_y) \leftarrow \mathcal{G}(s,t)$.
  $\mathbf{P}_s^r \leftarrow \mathbf{S}(\theta_x, \theta_y)(\mathbf{P}_s - \mathbf{c}_s\mathbf{1}^\top) + \mathbf{c}_s\mathbf{1}^\top$.
  Find nearest column for each column of $\mathbf{P}_s^r$ in the columns of $\mathbf{P}_s$ to find $\mathbf{\Pi}_s$.
  $\mathbf{C}(s,t) \leftarrow ||\mathbf{P}_s^r - \mathbf{P}_s\mathbf{\Pi}_s||_F$.
end for
$s^0, t^0 \leftarrow \underset{s,t}{\text{argmin}}\ \mathbf{C}$.
$(\theta_x^0, \theta_y^0) \leftarrow \mathcal{G}(s^0, t^0)$.

Output: Initial (θ_x^0, θ_y^0).

Fig. 5, we show the F-score for the proposed method as we vary the number of points (n_2) sampled uniformly at random for all the models in dataset [47]. We note that for $n_2 = 500$, the F-scores saturate. Therefore, we choose $n_2 = 500$ for the model. We present all the steps in Algorithm 1.

Robust Symmetry Detection. We know that the L2-norm loss is not robust to outliers as even one outlier can produce a wrong result. The L1-norm loss can tolerate up to 50% outliers, but it is not differentiable at zero. In order to make our approach robust to outliers, perturbations, and missing parts, we follow the trimming strategy: the truncated L2-norm [56]. We minimize the cost function below

$$\sum_{i=1}^{n} \min\left(\|\mathbf{S}(\mathbf{p}_i - \mathbf{c}) + \mathbf{c} - \mathbf{p}_j\|_2^2, \epsilon\right). \tag{10}$$

Let $\mathbf{P}_r = \mathbf{S}(\mathbf{P} - \mathbf{c}\mathbf{1}^\top) + \mathbf{c}\mathbf{1}^\top$. Then, we find the nearest column for each column of the matrix $\mathbf{P}_r$ in the columns of the matrix $\mathbf{P}$ to

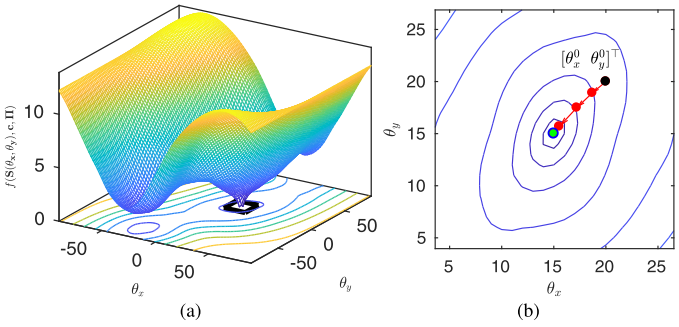

Fig. 6. Visualization of the initialization and the convergence. (a) The error function $f(\mathbf{S}, \mathbf{c}, \mathbf{\Pi})$ as we vary the rotation matrix parametrized by the rotation angles θ_x and θ_y about the x-axis and y-axis, perspectively. We observe that it is a non-linear and a non-convex function. (b) The zoomed contour map (black colored rectangle in (a)). The initial θ_x and θ_y shown as black colored point obtained by the proposed randomized algorithm.

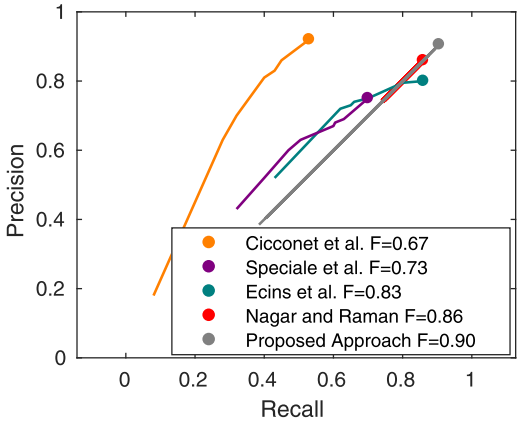

Fig. 7. Recall vs Precision curves comparisons for Cicconet et al. [15], Ecins et al.[13], Speciale et al. [1], Nagar and Raman [14], and the proposed approach on the dataset [47]. We report the maximum F-score in the legends and on the curve using a colored point.

find $\mathbf{\Pi}$. Let $\mathbf{Q} = \mathbf{P\Pi}$. Now, we can represent the ith error residual for each pair of reflective symmetric points as $e_i = \|\mathbf{p}_i^{\mathrm{r}} - \mathbf{q}_i\|_2^2$. We set ϵ equal to median$(e_1, \ldots, e_n)$ of the error residuals. We find the optimal $\mathbf{S}$ and $\mathbf{c}$ using the points for which $e_i \leq \epsilon$. We again update the matrix $\mathbf{\Pi}$ for all the points using the updated $\mathbf{S}$ and $\mathbf{c}$. We iteratively keep repeating this process until convergence. We stop when the change in the normal vector to the estimated reflection symmetry plane is less the 0.001° and the change in the point on the estimated $\mathbf{c}$ is less then 0.001. We present the complete procedure in Algorithm 2.

Algorithm 2 *Robust symmetry detection.*

Input: A point cloud $\mathcal{P}$ represented as a matrix $\mathbf{P} = \begin{bmatrix}\mathbf{p}_1 & \mathbf{p}_2 & \ldots & \mathbf{p}_n\end{bmatrix} \in \mathbb{R}^{3\times n}$.

Steps Involved:

1: Initialize the matrix $\mathbf{S}$ using Algorithm 1.
2: **for** $k \in \{1, 2, \ldots, 5\}$ **do**
3: $\quad \mathbf{P}_{\mathrm{r}} \leftarrow \mathbf{S}(\mathbf{P} - \mathbf{c}\mathbf{1}^\top) + \mathbf{c}\mathbf{1}^\top$.
4: $\quad$ Find nearest neighbor for each column of $\mathbf{P}_{\mathrm{r}}$ in the columns of $\mathbf{P}$ to find $\mathbf{\Pi}$.
5: $\quad \mathbf{Q} \leftarrow \mathbf{P\Pi}$.
6: $\quad e_i \leftarrow \|\mathbf{p}_i^{\mathrm{r}} - \mathbf{q}_i\|_2$, $\forall i \in [n]$.
7: $\quad \epsilon \leftarrow$ median$(e_1, \ldots, e_n)$.
8: $\quad$ Remove the ith columns of $\mathbf{P}$ and $\mathbf{P}_{\mathrm{r}}$ if $e_i > \epsilon$. Update $\mathbf{\Pi}$ as in step 4.
9: $\quad \mathbf{W} \leftarrow (\mathbf{P\Pi} - \mathbf{c}\mathbf{1}^\top)(\mathbf{P}^\top - \mathbf{1}\mathbf{c}^\top)$.
10: $\quad \mathbf{U\Sigma V}^\top \leftarrow \mathbf{W}$.
11: $\quad \mathbf{S} \leftarrow \mathbf{VU}^\top$.
12: $\quad \mathbf{c} \leftarrow$ solution of the linear system $(\mathbf{I} - \mathbf{S})\mathbf{c} = \frac{1}{2n}(\mathbf{I} - \mathbf{S})(\mathbf{SP1} + \mathbf{P\Pi 1})$.
13: **end for**

Output: Optimal $\mathbf{S}$, $\mathbf{t}$, and $\mathbf{\Pi}$.

In Fig. 6, we show the convergence for an example point cloud. In Fig. 6(a), we visualize the error function $f(\mathbf{S}, \mathbf{c}, \mathbf{\Pi})$ as we vary the rotation angles θ_x and θ_y. In Fig. 6(b), the initial θ_x and θ_y are shown as a black colored point obtained by the proposed randomized algorithm. We achieve the global solution denoted as the green colored point in about 5 iterations using the proposed approach.

6. Results and evaluation

6.1. Evaluation of reflection symmetry plane

In order to evaluate our method, we follow the procedure proposed in [47]. The dataset in [47] for single symmetric object contains 1354 3D models representing a symmetric object. We compare the performance of our approach with the performances of the state-of-the-art methods in [1,13,15], and [14] using the F-score metric proposed in [47]. We also compare the performance of our method with [15] and [14] to see the effect of outliers and perturbation along with the computational complexity. We find the precision vs recall curves and report the F-score. The precision is defined as $P = \frac{tp}{tp+fp}$, the recall is defined as $R = \frac{tp}{tp+fn}$, and the F-Score is defined as $F = \frac{2PR}{P+R}$. Here, $tp =$ the number of estimated symmetry planes which are correct, $fp =$ the number of estimated symmetry planes which are incorrect, and $fn =$ the number of ground-truth symmetry planes which are not detected. In order to determine if a detected plane of reflective symmetry is correct or incorrect, we follow the same procedure as that of [47], which is stated as follows. Let $\mathbf{p}_1^{\mathrm{e}}$, $\mathbf{p}_2^{\mathrm{e}}$, and $\mathbf{p}_3^{\mathrm{e}}$ be three points on the estimated symmetry plane and $\mathbf{p}_1^{\mathrm{g}}$, $\mathbf{p}_2^{\mathrm{g}}$, and $\mathbf{p}_3^{\mathrm{g}}$ be three points on the ground truth symmetry plane. These three points are the points of intersection of the symmetry plane with the bounding box of the symmetric object. Then, the estimated symmetry plane is correct if the angle between the normals of the estimated plane $\mathbf{n}^{\mathrm{e}} = (\mathbf{p}_1^{\mathrm{e}} - \mathbf{p}_2^{\mathrm{e}}) \times (\mathbf{p}_1^{\mathrm{e}} - \mathbf{p}_3^{\mathrm{e}})$ and the ground truth plane $\mathbf{n}_{\mathrm{g}} = (\mathbf{p}_1^{\mathrm{g}} - \mathbf{p}_2^{\mathrm{g}}) \times (\mathbf{p}_1^{\mathrm{g}} - \mathbf{p}_3^{\mathrm{g}})$ is less than a threshold angle. Furthermore, the distance of the center of the estimated plane $\mathbf{c}_{\mathrm{e}} = \frac{\mathbf{p}_1^{\mathrm{e}} + \mathbf{p}_2^{\mathrm{e}}}{2}$ from the ground truth symmetry plane is below a given threshold τ_d. We vary the angle threshold $\tau_\theta \in [0, 45^\circ]$ and the distance threshold $\tau_d \in [0, 2w]$, where, $w = \min\{\|\mathbf{p}_1^{\mathrm{e}} - \mathbf{p}_2^{\mathrm{e}}\|_2, \|\mathbf{p}_1^{\mathrm{e}} - \mathbf{p}_3^{\mathrm{e}}\|_2, \|\mathbf{p}_1^{\mathrm{g}} - \mathbf{p}_2^{\mathrm{g}}\|_2, \|\mathbf{p}_1^{\mathrm{g}} - \mathbf{p}_3^{\mathrm{g}}\|_2\}$. In Fig. 7, we show the obtained recall vs precision curves for the state-of-the-art approaches in [1,13–15], and the proposed approach on the dataset in [47] for single reflective symmetry plane. We report the maximum F-score in the legends using a colored point. We achieve the state-of-the-art performance on the dataset in [47]. In Fig. 8, we show the detected plane of reflective symmetry on a few models from the dataset [47]. Our method can detect symmetry real objects using their partial scans as well as in presence of significant amount the background points. For example consider the raw scans shown in Fig. 9.

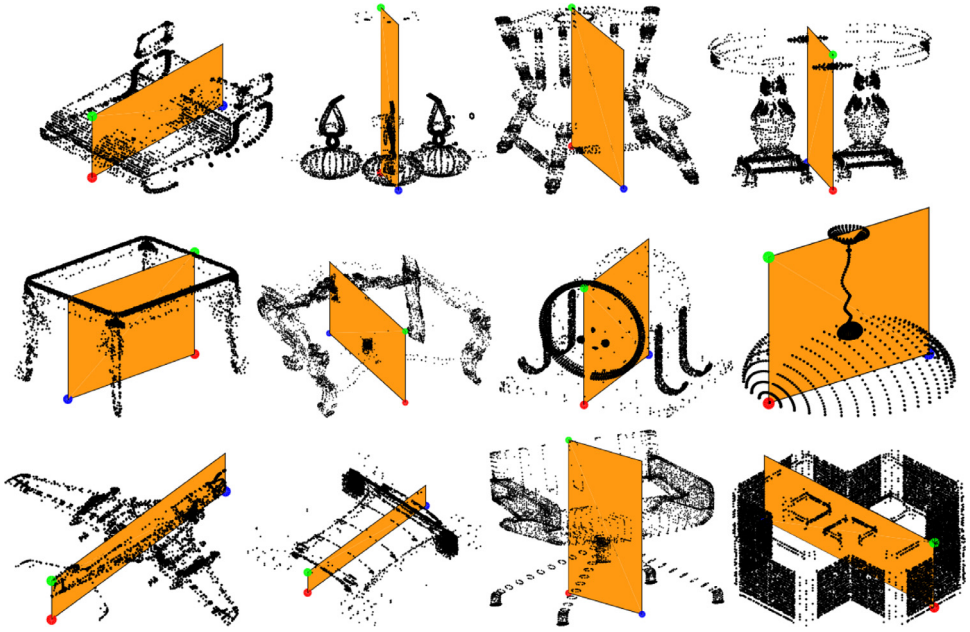

Fig. 8. The detected plane of reflective symmetry on a few models from the dataset in [47].

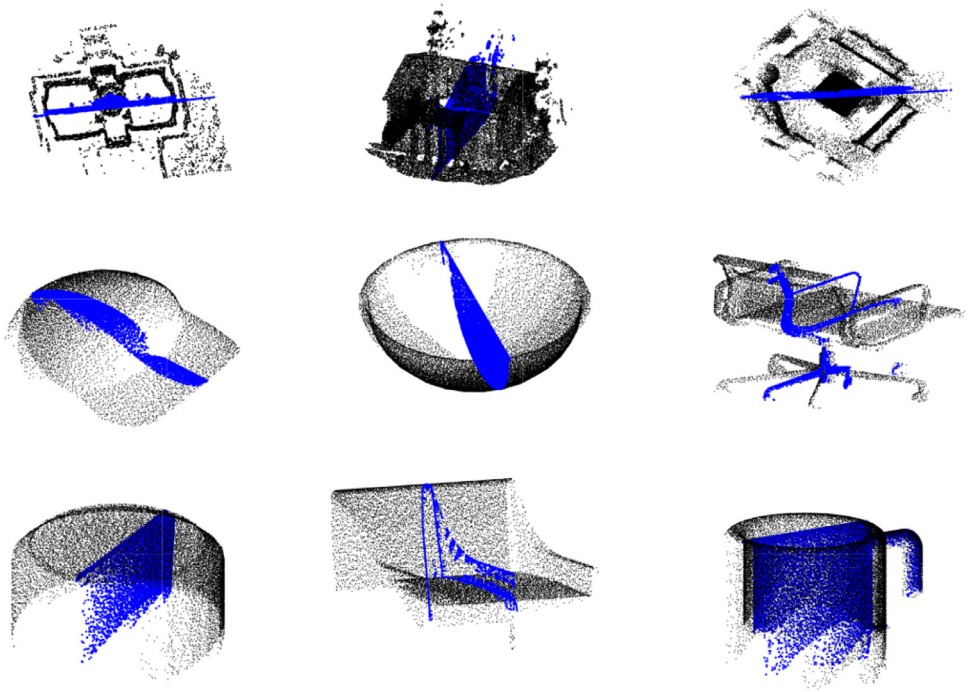

Fig. 9. A few example of the detected symmetries in scans of real objects. The first two objects are from the dataset [1] and other objects are from a RGBD dataset [57]. Here, the blue colored points represents the mid point of line segment joining two reflective symmetric points. We observe that our method is able to detect symmetry in the partial scans. (For interpretation of the references to colour in this figure legend, the reader is referred to the web version of this article.)

6.2. Evaluation on partial real scans

In order to test the performance of the proposed approach, we evaluate the performance on partial scans of real-world objects. For this, we compare the proposed approach with the performance of that of the state-of-the-art approach proposed in [14]. For this purpose, we use the benchmark dataset provided in [47]. This dataset contains 20 partial scans of real-world objects with the ground-truth symmetry plane available. In order to compare the performance of the proposed approach with the performance of the method proposed in [14], we use the same evaluation as discussed in Section 6.1. The average *F*-Score for the proposed is equal to 0.87 and the *F*-score for the method proposed in [14] is equal to 0.72. In Fig. 10, we show a few examples of the results of the proposed approach on the partial scans of real world objects from the dataset provided in [47].

6.3. Effect of outliers

We perform the following experiment to analyze the performance of our approach in the presence of outliers. We add random noise to the input 3D model to get the noisy model $\mathcal{P}^{\text{new}} =$

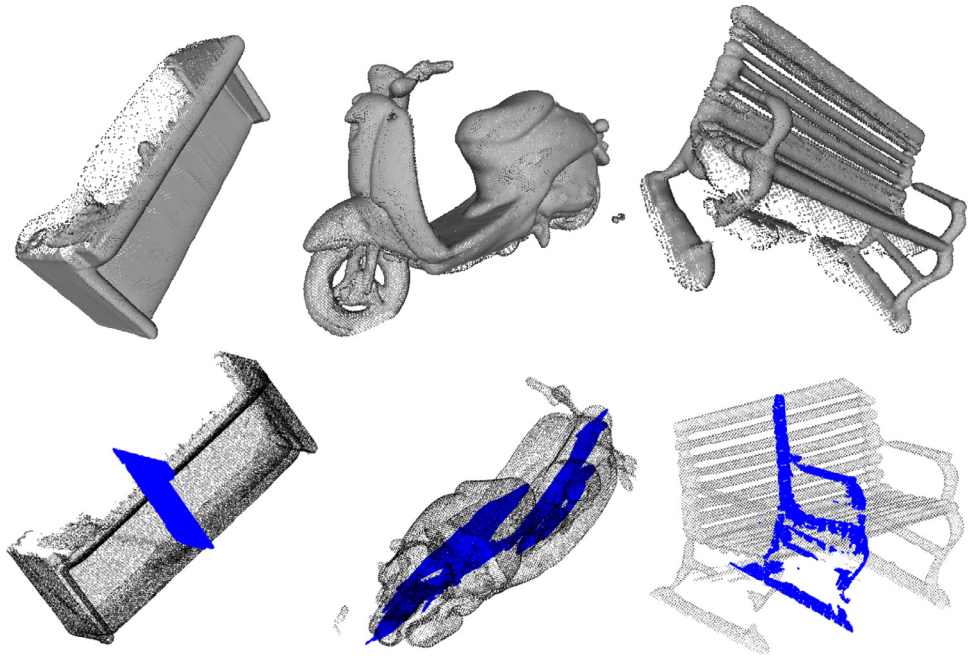

Fig. 10. The detected plane of reflective symmetry on a few scans of the real world objects from the dataset in [47] using the proposed approach.

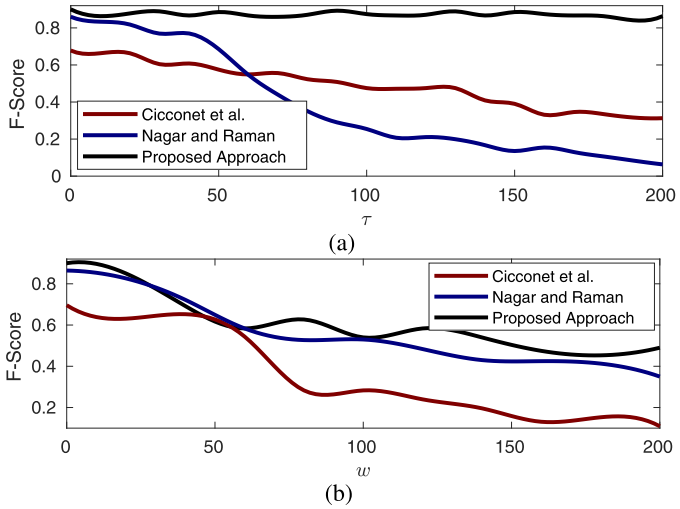

Fig. 11. Robustness to the outliers and the perturbation on the models from the dataset in [47] compared with the methods in [15] and [14]. (a) The τ vs the *F*-score. (b) The w vs the *F*-score.

$\mathcal{P} \cup \mathcal{P}^{\text{random}}$. Here, $\mathcal{P}^{\text{random}}$ is a set of noise points and we choose different number of noise points such that $|\mathcal{P}^{\text{random}}| = \tau|\mathcal{P}|/100$. We chose $\tau \in \{0, 10, \ldots, 200\}$. Each point $\mathbf{p}_i^{\text{r}}$ in the set $\mathcal{P}^{\text{random}}$ is a random vector such that

$$\mathbf{p}_i^{\text{r}} = \begin{bmatrix} 2(x_{\text{mx}} - x_{\text{mn}})r_{\text{x}} - 2x_{\text{mn}} \\ 2(y_{\text{mx}} - y_{\text{mn}})r_{\text{y}} - 2y_{\text{mn}} \\ 2(z_{\text{mx}} - z_{\text{mn}})r_{\text{z}} - 2z_{\text{mn}} \end{bmatrix}. \tag{11}$$

Here, r_{x}, r_{y}, and r_{z} are three independent random variables in the range [0,1]. x_{mx} and x_{mn} are the maximum and the minimum values of the x-coordinates for the input models. For each random $\mathcal{P}^{\text{new}}$, we measure the *F*-score for the methods in [14,15], and the proposed method. We perform this experiment on the dataset in [47] by randomly sampling 1000 points from each model so that we can compare with the method in [14]. In Fig. 11(a), we plot the number of outliers τ (% of number of input points) vs the *F*-score. We observe that even if 2/3rd of the points are outliers, the *F*-score only drops from 0.90 to 0.85 for our approach. Whereas, the *F*-score drops from 0.67 to 0.36 for the method in [15]. In Fig. 12, we show the detected plane of reflective symmetry and the correspondences between the reflective symmetric points for $\tau = \{0, 100, 200\}$.

6.4. Effect of perturbation.

We perform the following experiment to analyze the performance of our approach after perturbation of each point of the model. We perturb each point $\mathbf{p}_i = \begin{bmatrix} x_i & y_i & z_i \end{bmatrix}^\top$ as $\mathbf{p}_i^{\text{new}} = \mathbf{p}_i + \mathbf{p}^{\text{random}}$. Here, we define

$$\mathbf{p}^{\text{random}} = \begin{bmatrix} r\sin(\theta_1)\cos(\phi_1) & r\sin(\theta_1)\sin(\phi_1) & r\cos(\theta_1) \end{bmatrix}^\top. \tag{12}$$

Here, $r \sim \mathcal{U}(0, h)$, $\theta_1 \sim \mathcal{U}(0, \pi)$, and $\phi_1 \sim \mathcal{U}(0, 2\pi)$ are three uniform random variables. We choose different values of $h = w \times \min(x_{\text{mx}} - x_{\text{mn}}, y_{\text{mx}} - y_{\text{mn}}, z_{\text{mx}} - z_{\text{mn}})/100$. Here, $w \in \{0, 20, \ldots, 200\}$. We perform this experiment on the dataset in [47] by randomly sampling 1000 points from each model so that we can compare with the method in [14]. In Fig. 11(b), we plot the perturbation radius w (% of number of input points) vs the *F*-score. We observe that even if $w = 200$, the *F*-score only drops from 0.90 to 0.56. However, for the method in [15], it reaches till 0.05. In Fig. 13, we show the detected planes and the correspondences between symmetric points for $w \in \{0, 100, 200\}$.

6.5. Effect of missing parts

We perform the following experiment to analyze the performance of our approach after removing some parts from the input model. We remove a subset of points $\mathcal{P}_{\text{r}}$ from the input set $\mathbf{P}$ such that $|\mathcal{P}_r| = \eta|\mathcal{P}|$, where $\eta \in \{0, 0.15, 0.28\}$. For each η, we calculate the *F*-score. Again, we use the dataset in [47] to perform this experiment. In Fig. 14, we show the detected plane of reflection symmetry and the correspondences between the reflective symmetric points for an example model. We get the same

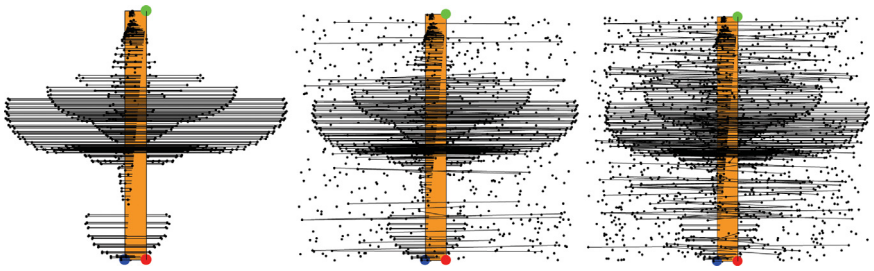

Fig. 12. Robustness to the outliers in a model from the dataset in [58]. The detected plane of reflective symmetry and correspondences between reflective symmetric points for $\tau = \{0, 100, 200\}$.

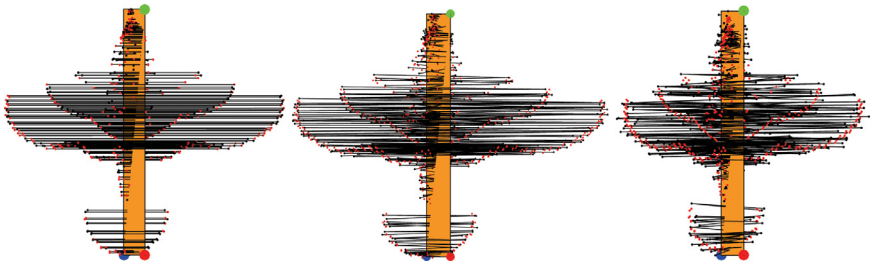

Fig. 13. Robustness to the perturbation to each point of the input model from the dataset in [58]. The detected plane of symmetry and correspondences between reflective symmetric points for $w \in \{0, 100, 200\}$. Actual points are colored black and the perturbed points are colored red. (For interpretation of the references to colour in this figure legend, the reader is referred to the web version of this article.)

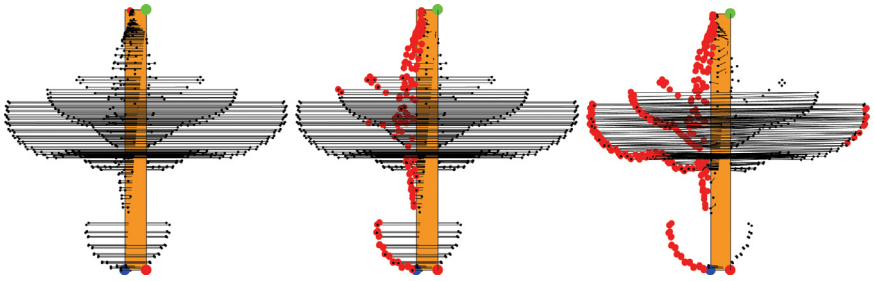

Fig. 14. Robustness to the missing parts in a model from the dataset in [58]. The detected plane and correspondences between the reflective symmetric points for $\eta \in \{0, 0.15, 0.28\}$. Red points denote the removed points.

behavior for the methods [14,15], and the proposed approach as that of the case for outlier points. The reason is that, if a part is missing, then the points corresponding to the mirror part will be outliers.

6.6. Computation time

The method in [15] takes 2060 s to compute symmetry in all 1354 models of the dataset in [47] and takes on an average 1.52 s for each model with an average number of vertices equal to 30,000. The method in [14] solves an Integer Linear Program (which takes $O(n^{3.5})$ time) and it would take lots of time to find symmetry in a model with an average number of vertices equal to 30,000. It takes around 38.5 s even for a model with a number of vertices equal to 500. We were not able to solve the integer linear program for $n = 30,000$ in our system. Our algorithm takes 866 s to compute symmetry in all 1354 models of the dataset in [47] and takes on an average of 0.63 s for each model with an average number of vertices equal to 30,000. We do this comparison on a Linux machine with i7 processor with 2.7 GHz frequency using MATLAB 17.

7. Conclusion

We have proposed a robust approach to find the global reflection symmetry of the symmetric 3D object with missing parts and containing by outlier points. We have posed the problem of detecting the reflection symmetry as an optimization problem which is a non-convex and a non-linear problem. We have proposed a fast randomized algorithm to find the approximate reflection symmetry for initialization to solve the non-convex problem. We have provided a closed-form solution for the problem of detecting the plane of reflection symmetry.

We have achieved state-of-the-art performance on a standard dataset and have shown that the proposed approach is robust to outliers, perturbation in each point of the symmetric object, and missing parts of the symmetric object. Another advantage of the proposed approach is that the proposed approach is independent of any feature descriptors which makes it applicable to any form of the input data such as point clouds sampled from the surface of a symmetric object and the volumetric point clouds. Our approach is applicable to the single reflective symmetric object. We would like to extend the proposed framework for detecting the multiple 3D reflection symmetries.

We believe that the high accuracy of our algorithm would enable applications such as 3D surface reconstruction [1], model completion [1,2], symmetrization [4], model reduction [5], 3D model reconstruction from single image [6], and viewpoint selection [12] as they will acquire better accuracy.

Declaration of Competing Interest

We wish to confirm that there are no known conflicts of interest associated with this publication and there has been no significant financial support for this work that could have influenced its outcome. We confirm that the manuscript has been read and approved by all named authors and that there are no other persons who satisfied the criteria for authorship but are not listed. We further confirm that the order of authors listed in the manuscript has been approved by all of us. We confirm that we have given due consideration to the protection of intellectual property associated with this work and that there are no impediments to publication, including the timing of publication, with respect to intellectual property. In so doing we confirm that we have followed the regulations of our institutions concerning intellectual property.

Acknowledgment

Shanmuganathan Raman was supported by an SERB IMPRINT-2 grant - IMP/2018/000250.

References

[1] P. Speciale, M.R. Oswald, A. Cohen, M. Pollefeys, A symmetry prior for convex variational 3d reconstruction, in: European Conference on Computer Vision, Springer, 2016, pp. 313–328.
[2] S. Thrun, B. Wegbreit, Shape from symmetry, in: IEEE International Conference on Computer Vision, vol. 2, IEEE, 2005, pp. 1824–1831.
[3] K. Xu, H. Zhang, A. Tagliasacchi, L. Liu, G. Li, M. Meng, Y. Xiong, Partial intrinsic reflectional symmetry of 3d shapes, ACM Trans. Graph. (TOG) 28 (5) (2009) 1–10.
[4] N.J. Mitra, L.J. Guibas, M. Pauly, Symmetrization, ACM Trans. Graph. (TOG) 26 (3) (2007) 63.
[5] N.J. Mitra, L.J. Guibas, M. Pauly, Partial and approximate symmetry detection for 3d geometry, in: ACM Transactions on Graphics (TOG), vol. 25, ACM, 2006, pp. 560–568.
[6] S.N. Sinha, K. Ramnath, R. Szeliski, Detecting and reconstructing 3d mirror symmetric objects, in: European Conference on Computer Vision, Springer, 2012, pp. 586–600.
[7] P. Simari, E. Kalogerakis, K. Singh, Folding meshes: hierarchical mesh segmentation based on planar symmetry, in: Eurographics Symposium on Geometry Processing, 256, 2006, pp. 111–119.
[8] H. Fu, X. Cao, Z. Tu, D. Lin, Symmetry constraint for foreground extraction, IEEE Trans Cybern 44 (5) (2014) 644–654.
[9] R. Nagar, S. Raman, SymmSLIC: Symmetry aware superpixel segmentation, in: IEEE International Conference on Computer Vision Workshops, 2017, pp. 1764–1773.
[10] E. Saber, A.M. Tekalp, Frontal-view face detection and facial feature extraction using color, shape and symmetry based cost functions, Pattern Recognit. Lett. 19 (8) (1998) 669–680.
[11] A. Kuehnle, Symmetry-based recognition of vehicle rears, Pattern Recognit. Lett. 12 (4) (1991) 249–258.
[12] J. Podolak, P. Shilane, A. Golovinskiy, S. Rusinkiewicz, T. Funkhouser, A planar-reflective symmetry transform for 3d shapes, ACM Trans. Graph. (TOG) 25 (3) (2006) 549–559.
[13] A. Ecins, C. Fermuller, Y. Aloimonos, Detecting reflectional symmetries in 3d data through symmetrical fitting, in: IEEE International Conference on Computer Vision Workshops, 2017, pp. 1779–1783.
[14] R. Nagar, S. Raman, Detecting approximate reflection symmetry in a point set using optimization on manifold, IEEE Trans. Signal Process. 67 (6) (2019) 1582–1595.
[15] M. Cicconet, D.G. Hildebrand, H. Elliott, Finding mirror symmetry via registration and optimal symmetric pairwise assignment of curves: Algorithm and results, in: IEEE International Conference on Computer Vision Workshop, IEEE, 2017, pp. 1759–1763.
[16] Y. Liu, H. Hel-Or, C.S. Kaplan, Computational Symmetry in Computer Vision and Computer Graphics, Now publishers Inc, 2010.
[17] N.J. Mitra, M. Pauly, M. Wand, D. Ceylan, Symmetry in 3d geometry: extraction and applications, in: Computer Graphics Forum, vol. 32, Wiley Online Library, 2013, pp. 1–23.
[18] Y. Lipman, X. Chen, I. Daubechies, T. Funkhouser, Symmetry factored embedding and distance, in: ACM Transactions on Graphics (TOG), vol. 29, ACM, 2010, p. 103.
[19] K. Xu, H. Zhang, W. Jiang, R. Dyer, Z. Cheng, L. Liu, B. Chen, Multi-scale partial intrinsic symmetry detection, ACM Trans. Graph. (TOG) 31 (6) (2012) 181.
[20] H. Zabrodsky, S. Peleg, D. Avnir, Symmetry as a continuous feature, IEEE Trans. Pattern Anal. Mach. Intell. 17 (12) (1995) 1154–1166.
[21] P.T. Highnam, Optimal algorithms for finding the symmetries of a planar point set, Inf. Process. Lett. 22 (5) (1986) 219–222.
[22] B. Li, H. Johan, Y. Ye, Y. Lu, Efficient 3d reflection symmetry detection: aview-based approach, Graph. Models 83 (2016) 2–14.
[23] B. Combès, R. Hennessy, J. Waddington, N. Roberts, S. Prima, Automatic symmetry plane estimation of bilateral objects in point clouds, in: IEEE Conference on Computer Vision and Pattern Recognition, IEEE, 2008, pp. 1–8.
[24] Z. Shi, P. Alliez, M. Desbrun, H. Bao, J. Huang, Symmetry and orbit detection via lie-algebra voting, in: Computer Graphics Forum, vol. 35, Wiley Online Library, 2016, pp. 217–227.
[25] A. Martinet, C. Soler, N. Holzschuch, F.X. Sillion, Accurate detection of symmetries in 3d shapes, ACM Trans. Graph. (TOG) 25 (2) (2006) 439–464.
[26] A. Berner, M. Bokeloh, M. Wand, A. Schilling, H.-P. Seidel, A graph-based approach to symmetry detection., in: Volume Graphics, vol. 40, 2008, pp. 1–8.
[27] A. Cohen, C. Zach, S.N. Sinha, M. Pollefeys, Discovering and exploiting 3d symmetries in structure from motion, in: IEEE Conference on Computer Vision and Pattern Recognition, IEEE, 2012, pp. 1514–1521.
[28] R. Nagar, S. Raman, Revealing hidden 3-d reflection symmetry, IEEE Signal Process. Lett. 23 (12) (2016) 1776–1780.
[29] P.J. Besl, N.D. McKay, Method for registration of 3-d shapes, in: Sensor Fusion IV: Control Paradigms and Data Structures, vol. 1611, International Society for Optics and Photonics, 1992, pp. 586–607.
[30] S. Rusinkiewicz, M. Levoy, Efficient variants of the ICP algorithm, in: IEEE International Conference on 3-D Digital Imaging and Modeling, IEEE, 2001, pp. 145–152.
[31] R. Lasowski, A. Tevs, H.-P. Seidel, M. Wand, A probabilistic framework for partial intrinsic symmetries in geometric data, in: IEEE International Conference on Computer Vision, IEEE, 2009, pp. 963–970.
[32] D.M. Thomas, V. Natarajan, Multiscale symmetry detection in scalar fields by clustering contours, IEEE Trans. Vis. Comput. Graph. 20 (12) (2014) 2427–2436.
[33] M. Kazhdan, B. Chazelle, D. Dobkin, A. Finkelstein, T. Funkhouser, A reflective symmetry descriptor, in: European Conference on Computer Vision, Springer, 2002, pp. 642–656.
[34] M. Bokeloh, A. Berner, M. Wand, H.-P. Seidel, A. Schilling, Symmetry detection using feature lines, in: Computer Graphics Forum, vol. 28, Wiley Online Library, 2009, pp. 697–706.
[35] C. Sun, J. Sherrah, 3D symmetry detection using the extended gaussian image, IEEE Trans. Pattern Anal. Mach. Intell. 19 (2) (1997) 164–168.
[36] M. Ovsjanikov, J. Sun, L. Guibas, Global intrinsic symmetries of shapes, in: Computer graphics forum, vol. 27, Wiley Online Library, 2008, pp. 1341–1348.
[37] H. Wang, H. Huang, Group representation of global intrinsic symmetries, in: Computer Graphics Forum, vol. 36, Wiley Online Library, 2017, pp. 51–61.
[38] R. Nagar, S. Raman, Fast and accurate intrinsic symmetry detection, in: European Conference on Computer Vision (ECCV), 2018, pp. 417–434.
[39] I. Sipiran, R. Gregor, T. Schreck, Approximate symmetry detection in partial 3d meshes, in: Computer Graphics Forum, vol. 33, Wiley Online Library, 2014, pp. 131–140.
[40] V.G. Kim, Y. Lipman, X. Chen, T. Funkhouser, Möbius transformations for global intrinsic symmetry analysis, in: Computer Graphics Forum, vol. 29, Wiley Online Library, 2010, pp. 1689–1700.
[41] A.M. Bruckstein, D. Snaked, Skew symmetry detection via invariant signatures, Pattern Recognit. 31 (2) (1998) 181–192.
[42] C. Sun, Symmetry detection using gradient information, Pattern Recognit. Lett. 16 (9) (1995) 987–996.
[43] Z. Xiao, Z. Hou, C. Miao, J. Wang, Using phase information for symmetry detection, Pattern Recognit. Lett. 26 (13) (2005) 1985–1994.
[44] Y. Lei, K.C. Wong, Ellipse detection based on symmetry, Pattern Recognit. Lett. 20 (1) (1999) 41–47.
[45] W. Shen, X. Bai, Z. Hu, Z. Zhang, Multiple instance subspace learning via partial random projection tree for local reflection symmetry in natural images, Pattern Recognit. 52 (2016) 306–316.
[46] M. Cicconet, V. Birodkar, M. Lund, M. Werman, D. Geiger, A convolutional approach to reflection symmetry, Pattern Recognit. Lett. 95 (2017) 44–50.
[47] C. Funk, S. Lee, M.R. Oswald, S. Tsogkas, W. Shen, A. Cohen, S. Dickinson, Y. Liu, 2017 ICCV Challenge: detecting symmetry in the wild, in: IEEE International Conference on Computer Vision Workshops, 2017, pp. 1692–1701.
[48] G. Loy, J.-O. Eklundh, Detecting symmetry and symmetric constellations of features, in: European Conference on Computer Vision, Springer, 2006, pp. 508–521.
[49] D.C. Hauagge, N. Snavely, Image matching using local symmetry features, in: IEEE Conference on Computer Vision and Pattern Recognition, IEEE, 2012, pp. 206–213.
[50] M. Chertok, Y. Keller, Spectral symmetry analysis, IEEE Trans. Pattern Anal. Mach. Intell. 32 (7) (2010) 1227–1238.
[51] Z. Wang, Z. Tang, X. Zhang, Reflection symmetry detection using locally affine invariant edge correspondence, IEEE Trans. Image Process. 24 (4) (2015) 1297–1301.

[52] I.R. Atadjanov, S. Lee, Reflection symmetry detection via appearance of structure descriptor, in: European Conference on Computer Vision, Springer, 2016, pp. 3–18.
[53] M. Elawady, C. Ducottet, O. Alata, C. Barat, P. Colantoni, Wavelet-based reflection symmetry detection via textural and color histograms: algorithm and results, in: IEEE International Conference on Computer Vision Workshop, IEEE, 2017, pp. 1734–1738.
[54] O. Sorkine, M. Alexa, As-rigid-as-possible surface modeling, in: Symposium on Geometry processing, vol. 4, 2007, p. 30.
[55] K.S. Arun, T.S. Huang, S.D. Blostein, Least-squares fitting of two 3-d point sets, IEEE Transa. Pattern Anal. Mach.Intell. (5) (1987) 698–700.
[56] O. Enqvist, E. Ask, F. Kahl, K. Åström, Tractable algorithms for robust model estimation, Int. J. Comput. Vis. 112 (1) (2015) 115–129.
[57] K. Lai, L. Bo, D. Fox, Unsupervised feature learning for 3d scene labeling, in: 2014 IEEE International Conference on Robotics and Automation (ICRA), IEEE, 2014, pp. 3050–3057.
[58] P. Shilane, P. Min, M. Kazhdan, T. Funkhouser, The princeton shape benchmark, in: Shape Modeling Applications, IEEE, 2004, pp. 167–178.

Rajendra Nagar is an Assistant Professor in the department of Electrical Engineering at the Indian Institute of Technology Jodhpur, India. Before that, he was an Assistant Research Professor in Electrical Engineering at Indian Institute of Technology Gandhinagar, India. He received his B.Tech. degree from Indian Institute of Technology Jodhpur, India in 2013. He received his Ph.D. degree in Electrical Engineering from Indian Institute of Technology Gandhinagar, India. His research interests include Computer Vision, 3D Shape Analysis, and Computer Graphics. He was awarded the TCS Research Scholarship for the period 2015–2018. He was also awarded a gold medal for the best academic performance in B.Tech. Electrical Engineering at IIT Jodhpur, 2013.

Shanmuganathan Raman is the Jibaben Patel Chair in Artificial Intelligence and an Associate Professor in Electrical Engineering and Computer Science and Engineering at Indian Institute of Technology Gandhinagar, India. He obtained his M.Tech. and Ph.D. degrees from Indian Institute of Technology Bombay, India. His research interests include Computer Vision, Machine Learning, and Computer Graphics. He was awarded the Microsoft Research India Ph.D. Fellowship for the year 2007.